Seasonal aspects of the quasi-biennial oscillation in the Max Planck Institute Earth System Model and ERA-40

Thomas R. Krismer,[1,2] Marco A. Giorgetta,[1] and Monika Esch[1]

Received 22 August 2012; revised 15 February 2013; accepted 20 February 2013; published 18 June 2013.

[1] This study investigates seasonal modulations of the quasi-biennial oscillation (QBO) of the tropical stratosphere. For this purpose, the Max Planck Institute Earth System Model (MPI-ESM), which internally generates a realistic QBO compared to the ERA-40 data set, is employed. The modeled QBO is forced with resolved and parametrized waves. At 5 hPa, the seasonal distribution of the onset of QBO westerly jets clusters in spring and fall due to the coupling of the QBO and the semiannual oscillation. This seasonal clustering of the westerly jets extends throughout the stratosphere, shifting to later months with increasing pressure. QBO westerly jets starting in the upper stratosphere in fall propagate to the middle stratosphere more slowly than westerly jets starting in spring. This is attributed to seasonal modulations of the QBO forcing and enhanced wave filtering by the QBO westerly jet in the lower stratosphere in fall and winter compared to spring and summer. The observed stalling of the QBO easterly jet in the lower stratosphere and the accompanied prolonged persistence of the QBO westerly jet in the vicinity of the tropopause are attributed equally to seasonal variations of the resolved and parameterized wave forcing and the advective forcing.

Citation: Krismer, T. R., M. A. Giorgetta, and M. Esch (2013), Seasonal aspects of the quasi-biennial oscillation in the Max Planck Earth System Model and ERA-40, *J. Adv. Model. Earth Syst.*, *5*, 406–421, doi:10.1002/jame.20024.

1. Introduction

[2] In the tropical stratosphere, the variability of the zonal mean zonal wind is dominated by the well known Quasi Biennial Oscillation (QBO). It manifests most clearly in the oscillation of westerly and easterly jets which originate in the upper stratosphere, propagate downwards to the vicinity of the tropical tropopause and alternate with a quasi-biennial period between 22 and 34 months [*Baldwin et al.*, 2001]. For this paper, a global climate model internally generating a realistic QBO is applied to investigate seasonal aspects of the QBO, namely, the coupling of the QBO to the semiannual oscillation in the vicinity of the stratopause, the clustering of the QBO phase onsets at specific times of the year as a function of altitude and the seasonal modulation of the propagation rates of the QBO jets.

[3] In observational data, *Dunkerton and Delisi* [1985] and *Dunkerton* [1990] found that the onsets of the westerly and easterly jets of the QBO at 50 hPa have a seasonal preference, both clustering in northern hemisphere spring and summer. At higher altitudes, the preferred season shifts to earlier months [*Dunkerton*, 1990; *Anstey and Shepherd*, 2008]. The month a QBO jet starts at a specific level is related to the month of the year the jet began in the upper stratosphere and the rate at which it propagates downward. *Wallace et al.* [1993], *Hamilton and Hsieh* [2002], and *Lu et al.* [2009] documented that integrated from 10 to 70 hPa, the QBO phases progress more rapidly in boreal winter and spring than in summer and fall. Between 30 and 50 hPa the descent of the easterly jet often slows down, and easterly and westerly jets stall for several months from July to February [*Naujokat*, 1986; *Dunkerton*, 1990; *Pascoe et al.*, 2005].

[4] In idealized numerical studies, seasonal variations of the QBO phase propagation have been related to a seasonal cycle of the equatorial upwelling [*Kinnersley and Pawson*, 1996; *Hampson and Haynes*, 2004]. Seasonal variations of the equatorial- and gravity wave activity and hence, the QBO momentum sources, also have the potential to alter the propagation rates [*Dunkerton*, 1990]. Such variations have been observed by *Allen and Vincent* [1995], *Fritts and Alexander* [2003], and *Li et al.* [2010], but their influence on the QBO has not been investigated further.

[5] Another interaction of the annual cycle with the QBO emerges from the interaction of the quasi-biennial oscillation and the semiannual oscillation (SAO) that occurs directly above the QBO. In the original theory of

[1]Max Planck Institute for Meteorology, Hamburg, Germany.
[2]International Max Planck Research School on Earth System Modelling (IMPRS), Hamburg, Germany.

1942-2466/13/10.1002/jame.20024

the QBO presented by *Lindzen and Holton* [1968], the SAO provides the westerly shear in the upper stratosphere, which is needed for effective deposition of westerly momentum by atmospheric waves. *Holton and Lindzen* [1972] introduced radiative wave damping as a dissipation mechanism for vertically propagating waves and found that the SAO was no longer needed to create the QBO. *Plumb* [1977] showed that in such a model, however, the evolution of the mean flow at any particular level is independent of what happens above, and downward influence is impossible if vertical diffusion is negligible. Numerical studies [*Gray and Pyle*, 1989; *Dunkerton and Delisi*, 1997; *Mayr et al*., 2010] illustrated the evolution of a QBO-like wave driven oscillation with and without a coupling to the SAO. *Kuai et al*. [2009] identified the initialization of QBO westerly jets by the SAO in the ERA-40 data set.

[6] From the seasonal aspects of the QBO discussed above, the following questions discussed in this paper arise:

[7] 1. How does the interaction of the QBO and the SAO influence the phase alignment of the QBO jets in the upper stratosphere and how does this phase alignment project to lower altitudes?

[8] 2. How does the seasonal stalling of the QBO jets in the lower stratosphere influence the propagation rates of the jets in the upper stratosphere?

[9] 3. How do seasonal variations of the equatorial wave forcing and the tropical upwelling contribute to variations of the propagation rates of the QBO jets?

[10] To explain the interaction of the annual cycle with the QBO, it is necessary to understand its forcing mechanism. The QBO is driven by vertically propagating atmospheric waves which deposit easterly and westerly momentum due to radiative attenuation, critical layer absorption and wave breaking [*Lindzen and Holton*, 1968; *Holton and Lindzen*, 1972]. The wave attenuation is most effective where the zonal phase speed of a wave is close to the zonal wind speed. Waves which deposit their wave momentum around the zero wind line between easterly and westerly jets drive the zero wind line downwards, towards the wave sources. However, the tropical upwelling in the stratosphere, which is driven by extratropical wave activity, tends to move stratospheric air upwards, and thus works against the downward propagation of the QBO jets [*Dunkerton*, 1997]. Through a long history of observational and modeling studies, large scale equatorial and extratropical waves, small scale gravity waves and vertical advection are recognized as the main forcing factors of the QBO [*Baldwin et al*., 2001; *Giorgetta et al*., 2006; *Kawatani et al*., 2010; *Evan et al*., 2012].

[11] Most modeling studies addressing seasonal aspects of the QBO investigate the influence of a prescribed variation of the vertical velocities on QBO-like oscillations within simplified models [*Kinnersley and Pawson*, 1996; *Hampson and Haynes*, 2004]. In this respect, an investigation within the setting of a global climate model (GCM) is still missing. It is desirable to generate a realistic QBO within GCMs because of the influence of the QBO on the extratropical climate [*Holton and Tan*, 1980; *Hamilton and Hsieh*, 2002; *Anstey and Shepherd*, 2008]. GCMs embed the QBO into their global circulation where the variability of the resolved wave forcing and the equatorial upwelling is internally generated, and thus consistent with the simulated climate. This sets a realistic setting, within which variations of the QBO can be investigated.

[12] Over the last decade, global climate models have developed the skill to internally generate QBO-like oscillations [*Takahashi*, 1999; *Scaife et al*., 2000; *Giorgetta et al*., 2002; *Kawatani et al*., 2010]. High-vertical resolution is required to simulate a QBO [*Giorgetta et al*., 2006; *Kawatani et al*., 2010]. The number of GCMs generating a QBO is still limited, and modeled QBOs often show systematic biases in structure, amplitude or period. Nevertheless modeled QBOs result from the ability of models to capture the essential wave-meanflow interaction.

[13] The investigation of the annual modulation of the QBO presented here is based on a 500 year long simulation of the Max Planck Institute Earth System Model (MPI-ESM) which generates a realistic QBO. In section 2, a brief description of the climate model MPI-ESM is given. General aspects of the simulated QBO are discussed in section 3.1. Section 3.2 describes how the interaction of the QBO and the SAO influences the phase alignment of the QBO jets in the upper stratosphere. The influence of seasonal variations of the QBO forcing on the propagation of the QBO jets in the upper stratosphere and on the stalling of the QBO jets in the lower stratosphere are discussed in section 3.3 and 3.4. Section 3.5 discusses the phase alignment of the QBO jets in the middle stratosphere, and a summary is given in section 4.

2. Model, Experiment, and Methods

[14] This work makes use of the Max Planck Institute Earth System Model [*Giorgetta et al*., 2012a], which consists of the ECHAM6 atmospheric GCM [*Stevens et al*., 2012], the JSBACH land vegetation model [*Raddatz et al*., 2007] and the MPIOM ocean GCM [*Marsland et al*., 2003] including the HAMOCC ocean bio-geochemistry model. For brevity, the generic name MPI-ESM is used in the following text. Here, the MPI-ESM-MR configuration is used, where "MR" designates the resolution of atmosphere and ocean GCMs. The ocean model makes use of a tripolar grid with a nominal resolution of 0.4°. The vertical grid has 40 z levels. The atmospheric component ECHAM6 is the direct successor of MAECHAM5, which is capable of internally generating a realistic QBO in terms of its periodicity, amplitude and vertical and latitudinal structure [*Giorgetta et al*., 2002, 2006; *Peña Ortiz et al*., 2008, 2010]. ECHAM6 generates an equally realistic QBO as MAECHAM5. In the "MR" configuration, ECHAM6 uses a spectral truncation at wave number 63 and an associated Gaussian grid of approximately 1.9° resolution in longitude and

latitude. The vertical grid has 95 hybrid sigma pressure levels resolving the atmosphere from the surface up to the center of the uppermost layer at 0.01 hPa. The top-of-the-model pressure is defined as 0 hPa. This grid has a nearly constant vertical resolution of 700 m from the upper troposphere to the middle stratosphere, and the resolution is better than 1 km at the stratopause. Thus the vertical grid is overall comparable to that used by *Giorgetta et al*. [2006] with respect to the vertical resolution in the QBO domain.

[15] The parameterization of subgrid scale convection, which is known to influence the resolved wave field, follows the Tiedtke-Nordeng scheme [*Tiedtke*, 1989; *Nordeng*, 1996]. ECHAM6 includes the Hines parameterization for nonorographic gravity waves [*Hines*, 1997a, 1997b]. The parametrized wave source is at 700 hPa. The source spectrum of the Hines parameterization follows the MAECHAM5 standard setting [*Manzini and McFarlane*, 1998; *Manzini et al*., 2006]. However, the otherwise constant wave-induced horizontal wind perturbations (rms winds) increase linearly from 1 to 1.2 m/s over 10°N to 5°N (10°S to 5°S). From 5°N to 5°S, the rms winds are constant at 1.2 m/s. The modification of the Hines parameterization was necessary to obtain a realistic QBO in MPI-ESM, where ECHAM6 is coupled to an ocean model. In MPI-ESM, the increase of the rms winds results in a four times larger wave momentum deposition in the domain of the QBO, given comparable wind profiles and wind shear in the stratosphere. *Giorgetta et al*. [2006] showed that increasing (decreasing) the rms winds in MAECHAM5 by 10 % strengthens (weakens) the QBO westerly jets and reduces (increases) the period. With an idealized one dimensional model, *Scaife et al*. [2000] showed that the QBO period generally decreases with increasing parametrized wave sources. For MPI-ESM, the applied equatorial strengthening of the rms winds meets the need for technically simple changes of the parameterization and, as shown below, a realistic QBO. Given the lack of observational constraints on tropical gravity waves and considering that the mostly convective nonorographic wave sources, which the Hines scheme mimics, are more abundant in the tropics than in the extratropics, such an enhancement seems to be justified. The parametrized gravity wave sources are constant in time.

[16] MPI-ESM has been used for many CMIP5 simulations [*Taylor et al*., 2009], and an overview over the dynamics of the middle atmosphere in these simulations is given by *Schmidt et al*. [2012]. This study makes use of the preindustrial CMIP5 simulation, which is forced by 1850 conditions and was integrated over 500 years [*Giorgetta et al*., 2012b]. The 500 simulated years include 209 complete quasi-biennial cycles, which allows us to calculate sound statistics of the discussed QBO features.

[17] In this study, the forcing of the QBO jets will be discussed within the framework of the Transformed Eulerian Mean (TEM) equations [*Andrews et al*., 1987]. Within this framework, the zonally averaged momentum equation states:

$$\begin{aligned}\overline{u}_t = \overline{v}^*[f-(a\cos\phi)^{-1}(\overline{u}\cos\phi)_\phi]-\overline{w}^*\overline{u}_z \\ +(\rho_0 a\cos\phi)^{-1}\nabla\cdot F+\overline{X},\end{aligned} \tag{1}$$

where ρ_0 is the log-pressure height-dependent density, a is the Earth radius and φ and z are the latitude and the log-pressure height. $\overline{u}$ is the zonal mean zonal wind and $\overline{v}^*$ and $\overline{w}^*$ are the meridional and vertical residual mean winds. f is the Coriolis parameter ($f \equiv 2\Omega sin\phi$ and Ω is the rotation rate of the Earth). Subscripts φ, z and t denote the meridional, vertical and temporal derivatives. $\overline{X}$ represents unresolved forcing terms.

[18] The nonorographic gravity wave drag and horizontal and vertical diffusion contribute to $\overline{X}$. However, these terms have not been stored for the CMIP5 simulation presented here. Therefore, $\overline{X}$ is computed according to equation (1) as the difference of the total acceleration minus the sum of the advective terms and the resolved wave forcing. To investigate the composition of $\overline{X}$, the first 30 years of the MPI-ESM preindustrial run have been repeated and the parameterized wave drag and the diffusion terms have been stored. Comparing the forcing terms showed that the parameterized wave drag dominates the total residuum, thus making $\overline{X}$ a good approximation for the parameterized gravity wave drag.

[19] $\nabla\cdot$F denotes the vertical and meridional divergence of the Eliassen Palm Flux (EP-Flux), which is a measure of the transport and deposition of zonal momentum by atmospheric waves in the stratosphere [*Andrews et al*., 1987]. In this study, F denotes the EP-Flux carried by waves resolved in MPI-ESM-MR with global wave numbers k ranging from 0 to 63. To distinguish the contribution of easterly and westerly waves to the atmospheric wave forcing, the zonal wave number/frequency distribution of the EP-Flux is computed following *Horinouchi et al*. [2003]:

$$\begin{aligned}\frac{F^{(\phi)}(k,\omega)}{\rho_0 a\cos\phi} = \mathrm{RE}[\overline{u}_z\hat{v}(k,\omega)\hat{\theta}^*(k,\omega)/\overline{\theta}_z] \\ -\mathrm{RE}[\hat{u}(k,\omega)\hat{v}^*(k,\omega)],\end{aligned} \tag{2}$$

$$\begin{aligned}\frac{F^{(z)}(k,\omega)}{\rho_0 a\cos\phi} = \mathrm{RE}\left\{\left[f-\frac{(\overline{u}\cos\phi)_\phi}{a\cos\phi}\right]\hat{v}(k,\omega)\hat{\theta}^*(k,\omega)/\overline{\theta}_z\right\} \\ -\mathrm{RE}\{\hat{u}(k,\omega)\hat{w}^*(k,\omega)\}.\end{aligned} \tag{3}$$

[20] In equations (2) and (3), θ is the potential temperature. A hat denotes the Fourier coefficients of the variables, whereas an asterisk denotes the complex conjugate. The Fourier coefficients have been derived by applying a Fast Fourier Transform in longitude and time for each month of the simulation separately, each month having six hourly data output. There is no temporal overlap between the months. k and ω denote the zonal wave number and frequency. The acceleration of the mean flow due to resolved waves with a certain phase speed is derived by summing the divergence of the spectral EP-Flux over bins of the same ground

based phase speed c, which is related to k and ω via the relation $c(k, \omega)=\omega/k$:

$$\overline{u}_{t(\nabla\cdot F(c))}=\sum \frac{\nabla \cdot F(k,\omega)|_{\frac{\omega}{k}=c}}{\rho_0 a \cos\phi}. \quad (4)$$

[21] For the understanding of the QBO it is important to remember that the wave momentum deposition is strongest where the wind speed is close to the phase speed [*Lindzen and Holton*, 1968; *Dunkerton and Fritts*, 1984; *Fritts and Alexander*, 2003]. The shear layer associated with a stronger QBO jet includes a larger range of velocities than the shear layer of a weaker jet. Hence, a broader spectrum of waves with larger phase speeds meet their critical level within the stronger shear zone. To a certain degree, this results in stronger wave momentum deposition and stronger acceleration of the mean flow.

3. Results

3.1. The QBO in MPI-ESM

[22] Figures 1a and 1c show the monthly mean zonal mean zonal wind in the tropical stratosphere and lower mesosphere over a 15 year period of the 500 year long MPI-ESM simulation and from 1984 to 1998 in the ERA-40 reanalysis data set. Between 0.1 and 2 hPa, the easterly and westerly jets of the semiannual oscillation dominate the zonal wind field. Between 5 and 100 hPa, westerly and easterly jets alternate with a quasi-biennial period. The QBO in MPI-ESM has the same range of periods between 24 and 34 months and the same mean period of 28.8 months as the QBO in ERA-40.

[23] In MPI-ESM, the peak to peak amplitude of the QBO steadily increases from 100 to 10 hPa, where it reaches 70 m/s (Figure 1b). Compared to ERA-40, the maximal QBO amplitude is roughly 50% stronger and higher up in the stratosphere.

[24] Consistent with the ERA-40 data set, the semi annual oscillation becomes important above 7 hPa in MPI-ESM (Figure 1b). Again, in MPI-ESM, the peak amplitude of the SAO is stronger (50 compared to 40 m/s) and higher up in the stratosphere (1 compared to 2 hPa) than in ERA-40. Above 10 hPa, no wind observations are assimilated into the ERA-40 reanalysis system to constrain the QBO and the SAO, which then are internally generated above that altitude. However, *Baldwin and Gray* [2005] showed that the amplitude of the QBO in ERA-40 generally compares well to rocket- and rawisonde data, and that the QBO and the SAO are well represented up to 3 hPa. Based on this, the QBO and the SAO are too strong in MPI-ESM.

[25] The QBO dominates the stratospheric variability between 100 and 10 hPa, which is in accordance with ERA-40 (Figure 1d). The QBO explains about 90% of

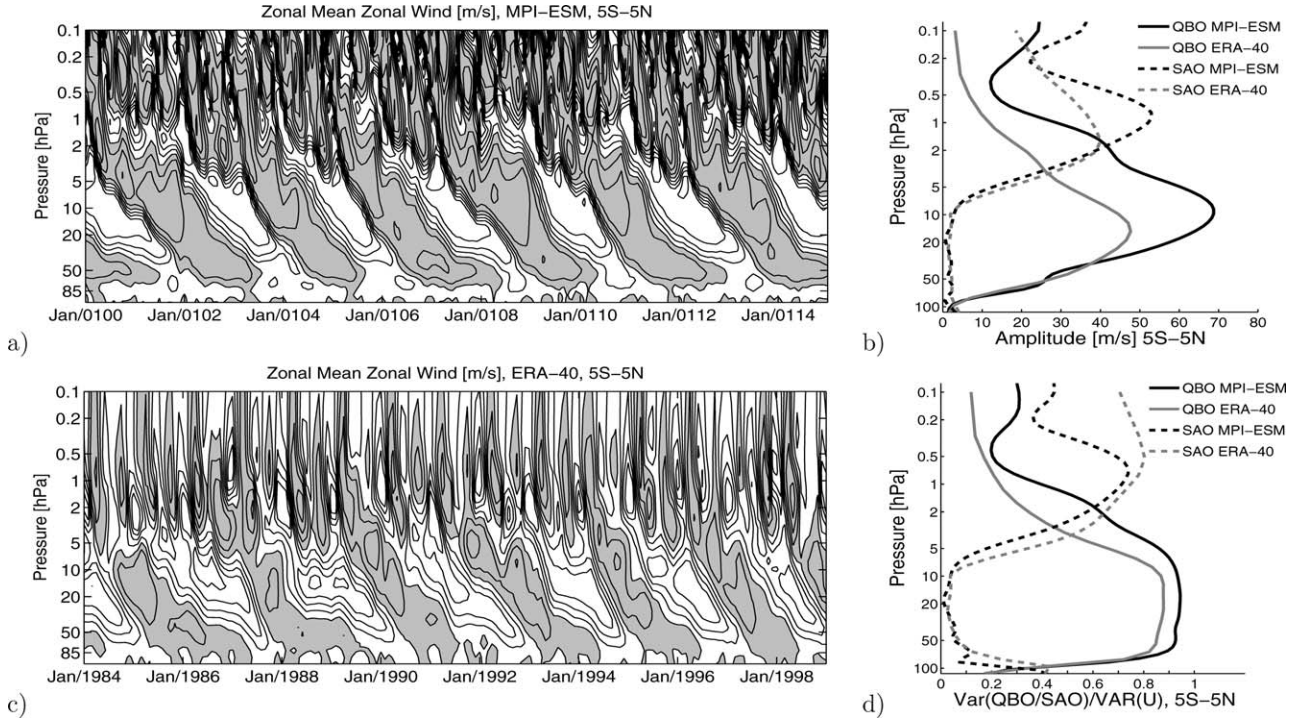

Figure 1. Time-height cross section of the zonal mean zonal wind in (a) MPI-ESM and (c) ERA-40. The contour interval is 10 m s^{-1}. Positive wind speeds are highlighted in gray. (b) Profiles of the peak to peak zonal wind amplitude of the QBO (solid) and the SAO (dashed) in MPI-ESM (black) and ERA-40 (gray). (d) Profiles of the zonal wind variance of the QBO (solid) and the SAO (dashed) relative to the total zonal wind variance in MPI-ESM

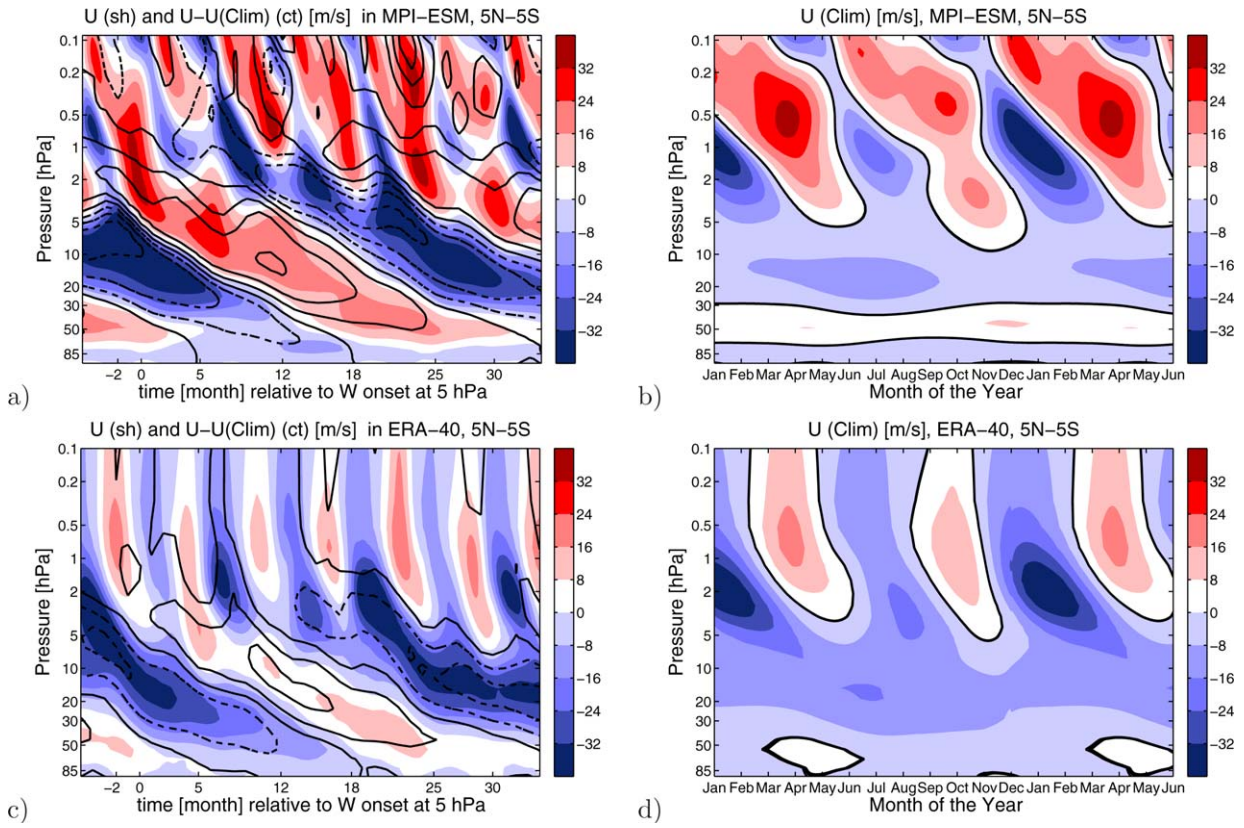

Figure 2. Time-height cross section of the composite of the zonal mean zonal wind U (shading) and the zonal wind after subtracting the annual climatology U-U(clim) (contours) in (a) MPI-ESM and (c) ERA-40. The contour interval is 10 m s^{-1}. The zero-wind line and positive wind speeds are solid, negative winds speeds are dashed. The central date (month 0) refers to the onset of the QBO westerly jets in the deseasonalized zonal wind at 5 hPa in May for MPI-ESM and in June for ERA-40. Time-height cross section of the climatological zonal mean wind U(clim) in (b) MPI-ESM and (d) ERA-40. The black line indicates the zero-wind line.

the variance of the zonal wind on the QBO core levels in MPI-ESM, but only about 80% in ERA-40 (Figure 1d). Because of the stronger QBO, the contribution of the SAO to the total variance is weaker in MPI-ESM than in ERA-40, except for a narrow region from 1 to 0.5 hPa, where the SAO is equally important in both data sets (Figure 1d). Above 0.5 hPa, the amplitude and the relative variance of the QBO increase in MPI-ESM due to the mesospheric QBO [*Peña Ortiz et al.*, 2010], which is not covered in ERA-40 (Figures 1b and 1d).

3.2. QBO/SAO Coupling

[26] The SAO and the QBO overlap above 5 hPa (Figure 1). The interaction between both oscillations is illustrated in Figures 2a and 2c, which show composites of the zonal mean zonal wind and the deseasonalized zonal mean zonal wind in MPI-ESM and ERA-40. The composites consist of only those quasi-biennial cycles where the onset of the westerly jet in the deseasonalized wind at 5 hPa (month 0) occurs in May for MPI-ESM and in June for ERA-40. These are the months when the onsets are most frequent in the respective data set (shown below).

[27] At 5 hPa, the deseasonalized and the full zonal wind coincide well in MPI-ESM, while in ERA-40, the QBO westerly jet starts 5 months earlier in the deseasonalized than in the full zonal wind (month 0 and 5 of Figure 2c). *Punge and Giorgetta* [2007] found that in ERA-40, the zonal wind speed is systematically weaker by 10m/s in the first half of the data set, probably due to a lower quality of the zonal wind observations during the early years of ERA-40. Deseasonalizing the full zonal wind partly removes the offset, which does not affect the QBO amplitude [*Punge and Giorgetta*, 2007].

[28] The QBO westerly jet in the zonal wind becomes weaker as it propagates from the upper stratosphere to lower altitudes (Figures 2a and 2c). It becomes more permeable for waves transporting westerly momentum, as fewer waves encounter their critical level, where the phase speed is close to the wind speed [*Ern et al.*, 2011; *Yang et al.*, 2012]. Thus, more westerly momentum can reach the upper stratosphere when a relatively weak QBO westerly jet exists in the lower stratosphere than when a stronger QBO westerly jet is in the middle stratosphere. Consequentially, the SAO westerly jet is forced more strongly and can propagate to lower altitudes in the stratosphere at times of a weaker and lower QBO westerly jet (Figure 2a, month 5, 12, 18 and 25). The same considerations are true for the SAO and QBO easterly jets. This dependence of the SAO on the QBO

is shown by MPI-ESM and ERA-40, and is in agreement with results from earlier observational and modeling studies [*Dunkerton and Delisi*, 1997; *Garcia et al.*, 1997; *Scaife et al.*, 2000; *Giorgetta et al.*, 2006; *Peña Ortiz et al.*, 2010].

[29] In MPI-ESM, the QBO is coupled to the SAO in such a way that at 5 hPa, every QBO westerly shear zone directly connects to a SAO westerly jet. A SAO westerly jet continues as a westerly jet of the QBO after every 4 to 6 semi annual cycles (month 0 and 29 in Figure 2a), when the westerly jet of the previous quasi-biennial cycle, located between 30 and 80 hPa in month 0 of Figure 2a, is weak and permeable for a sufficient amount of westerly waves.

[30] For ERA-40, Figure 2c shows that the westerly jet of the deseasonalized zonal wind (contours) starts at 5 hPa 5 months earlier than the jet in the actual zonal wind (shading). As found by *Dunkerton* [1997] and *Kuai et al.* [2009], the onsets of both jets coincide well with the descent of an SAO westerly phase. However, for the westerly jet of the actual zonal wind this is not always the case, as shown by the jet evolving at 5 hPa in 1985 and 1987 in Figure 1c (and a number of westerly jets in earlier years).

[31] In ERA-40, the amplitude of the SAO is larger than the amplitude of the QBO above 5 hPa (Figure 1b). In month 1–4 of Figure 2c between 5 and 1 hPa, the overlap of the QBO westerly phase in the deseasonalized wind with easterly winds in the actual wind illustrates that the SAO easterly jet masks the QBO westerly phase in the actual wind. Hence, the coupling of the QBO westerly jet to the SAO becomes more obvious when comparing the phase of the SAO with the onset of a QBO westerly jet in the deseasonalized zonal wind.

[32] The climatologies of the zonal wind in the stratosphere in MPI-ESM and ERA-40 are shown in Figures 2b and 2d. Both data sets show a seasonal asymmetry with a stronger semiannual cycle with maximal westerly winds at 0.5 hPa in March/April and a weaker semiannual cycle with maximal westerly winds at 0.5 hPa in September/October. This asymmetry is well observed and associated with stronger meridional momentum advection in boreal winter [*Delisi and Dunkerton*, 1988]. Also the composite in Figure 2a shows this asymmetry, as the SAO westerly jet at 0.5 hPa is stronger in April (month 11 and 23) than in October (month 17).

[33] A comparison of the zonal wind climatology and the seasonal distribution of the onset of QBO westerly jets in the upper stratosphere gives evidence of the initialization of the QBO westerly phase by SAO westerly jets. At 1 hPa in the simulation and the reanalysis data, the onset of the climatological SAO westerly jets occurs in mid February and mid August (Figures 2b and 2d). The jets reach 5 hPa some months later around May and October. These months mark the onset of a QBO westerly jet at 5 hPa if the SAO westerly jet continues its decent as a westerly jet of the QBO. This coupling displays in the seasonal distribution of the onsets of the QBO westerly jets in the upper stratosphere shown in Figure 3. In MPI-ESM, the onset of the 209 QBO westerly jets at 5 hPa occurs mainly in spring (April/May/June) and in fall (September/October/November), with two distinct peaks in May and in October and few occurrences from December to March (Figure 3a). In the deseasonalized zonal wind in MPI-ESM and

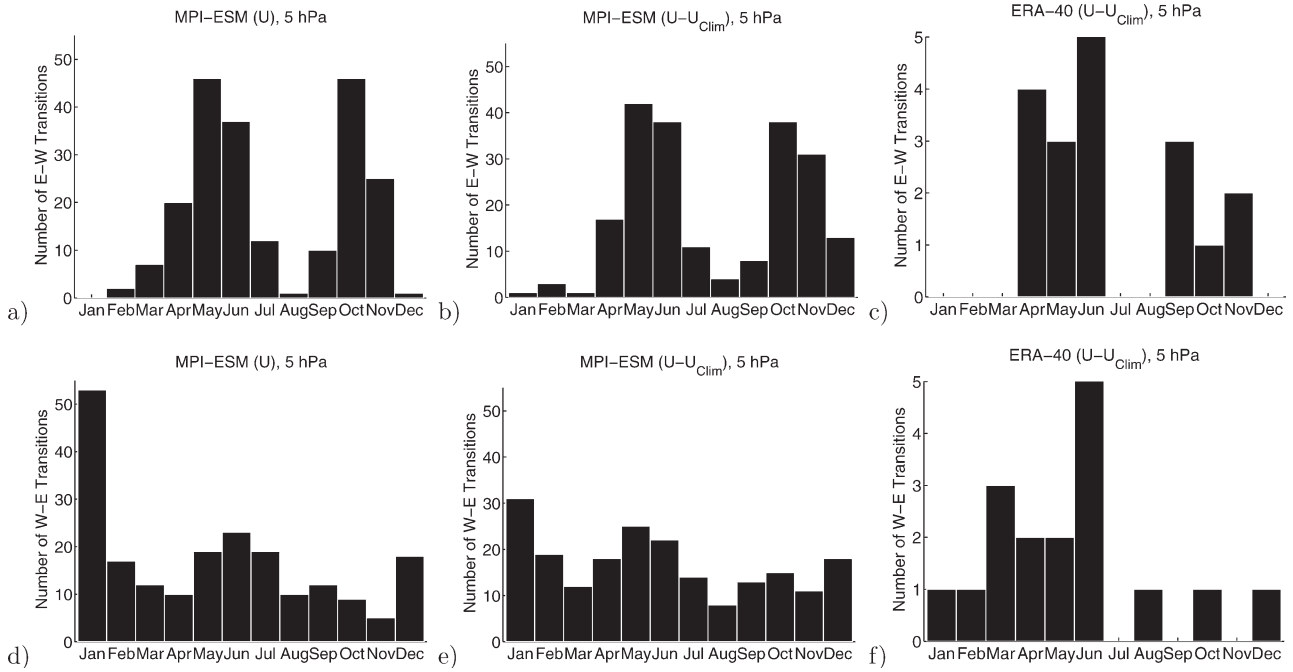

Figure 3. Monthly distribution of the onset of the QBO westerly (upper graph) and easterly jet (lower graph) at 5

ERA-40, the onset of the QBO westerly jet clusters at 5 hPa from April to June (Figures 3b and 3c). A second cluster extends from October to December in MPI-ESM and from September to November in ERA-40 (Figures 3b and 3c). This similar clustering illustrates the good agreement on the coupling of the onset of a QBO westerly phase to the descent of an SAO westerly jet between the model and the reanalysis data set.

[34] The seasonal distribution of the onset of the easterly jets at 5 hPa in MPI-ESM shows some clustering in December/January and from May to July (Figure 3d). During these months, the SAO is in its easterly phase at 5 hPa (Figure 2b). However, the distribution is much broader than the distribution of the onset of the westerly jets (Figure 3a). Although easterly jets are initiated and strengthened by the easterly phase of the SAO above 5 hPa, their occurrence is not limited to it. Once initiated, the easterly jets are not replaced by SAO westerly jets because the QBO westerly jet below filters the necessary westerly wave momentum flux (month 5 and 12 in Figure 2a). The easterly jet is sustained by weak easterly forcing, which increases during SAO easterly phases and as the QBO easterly jet in the lower stratosphere weakens [*Peña Ortiz et al*., 2010]. Because the easterly jet prevails continuously and not only during SAO easterly phases, it can pass 5 hPa and mark the onset of a QBO easterly jet throughout the year.

[35] In ERA-40, the onset of the deseasonalized easterly jets is confined to the period from January to June, contrary to the broad distribution shown by MPI-ESM (cf. Figures 3e and 3f). Subsampling successive 40 year long periods of the 500 year long MPI-ESM simulation revealed that there are periods when the distribution is more peaked. However, such periods are rare. Because of the weak seasonality of the onset of the QBO easterly jet in MPI-ESM, the focus of this study lies on the QBO westerly jet.

3.3. Propagation of QBO Jets through the Middle Stratosphere

[36] The different propagation characteristics of the QBO westerly jets starting at 5 hPa in spring and fall in MPI-ESM and ERA-40 are discussed next. Therefore, two composites of quasi-biennial cycles where the westerly jets pass 5 hPa either in April or May or in October or November are computed. For MPI-ESM, the actual zonal wind is considered for these composites, which include 66 and 71 samples in spring and fall, respectively. However, as noted in the discussion of Figure 2c, the QBO westerly jet of the actual wind in ERA-40 often is masked by an SAO easterly jet. Hence, in ERA-40 it is more convenient to create the composites based on the onset of the QBO westerly jet in the deseasonalized zonal wind, which include 7 and 3 samples for April/May and for October/November, respectively.

[37] Figure 4 shows the time-height cross section of the zonal mean zonal wind and its acceleration in the composites. Figures 4a and 4c shows that the QBO westerly jets starting at 5 hPa in spring propagate quickly to the middle stratosphere and the forcing along the zero-wind line, which separates the upper QBO westerly jet and the easterly jet below, is continuously high. However, westerly jets starting at 5 hPa in fall experience a period of almost zero acceleration at 7 hPa from December/January to February/March (Figures 4b and 4d), and hence, stall in their vertical propagation during this period. Thereafter, the mean flow acceleration increases again, and the westerly jet propagates to lower altitudes. Next, the cause of this stalling is discussed in the context of the momentum equation (equation (1)).

[38] In the GCM used for ERA-40, the QBO is generated through the assimilation process. An additional term enters the momentum balance (equation (1)) which accounts for the assimilation increments and which has not been reported. As the QBO does not emerge from the freely running model, it has to be doubted that the model generated terms of the momentum balance in ERA-40 are sufficient to drive the QBO. As such an investigation is beyond the scope of this study, the stratospheric momentum budget is discussed only for MPI-ESM.

[39] Figure 5 shows profiles of the zonal wind and the terms of equation (1) for MPI-ESM in month 2 of the composites of QBO westerly jets initiated in spring (labeled June/July) and fall (labeled December/January) in MPI-ESM. The zonal wind profiles in Figure 5 show an upper QBO westerly jet starting at 7 hPa, a lower-level QBO westerly jet with its core at 50 hPa and an easterly jet in between. Such a threefold wind profile has also been found by *Pascoe et al*. [2005]. Figure 5 illustrates that the stronger parameterized wave forcing and the stronger vertical momentum advection around 7 hPa (Figures 5c and 5d) are responsible for the stronger total forcing of the upper QBO westerly jet in June/July compared to December/February (Figure 5a, cf. Figures 4a and 4b). The difference in the advective forcing (Figure 5d) is due to the annual cycle of the equatorial upwelling. It is weak in June/July, when its extratropical Rossby-Waves forcing is low. Hence, in June/July the downward motion induced by the upper QBO westerly jet results in stronger momentum advection than in December/January (Figure 5d). Note that in MPI-ESM, the secondary circulation induced by the QBO westerly jet at high altitudes is strong enough to turn the generally upward equatorial vertical motion downwards, and the momentum advection is positive below the upper QBO westerly jet.

[40] In MPI-ESM, the parameterized wave sources are kept constant in time. Therefore, the difference of the parameterized wave forcing of the upper QBO westerly jet at 7 hPa in Figure 5c is due to stronger filtering of the parameterized waves between the wave sources at 700 hPa and the upper stratosphere in December/January compared to June/July. A part of this filtering is done by the QBO westerly jet in the lower stratosphere, located between 80 and 30 hPa in Figures 4 and 5 (called lower-level westerly jet hereafter). The lower-level westerly jet is stronger in December/January than in June/July (Figure 5). Hence, more parameterized westerly waves meet their critical level, where their phase speed is close to the zonal wind speed, and give

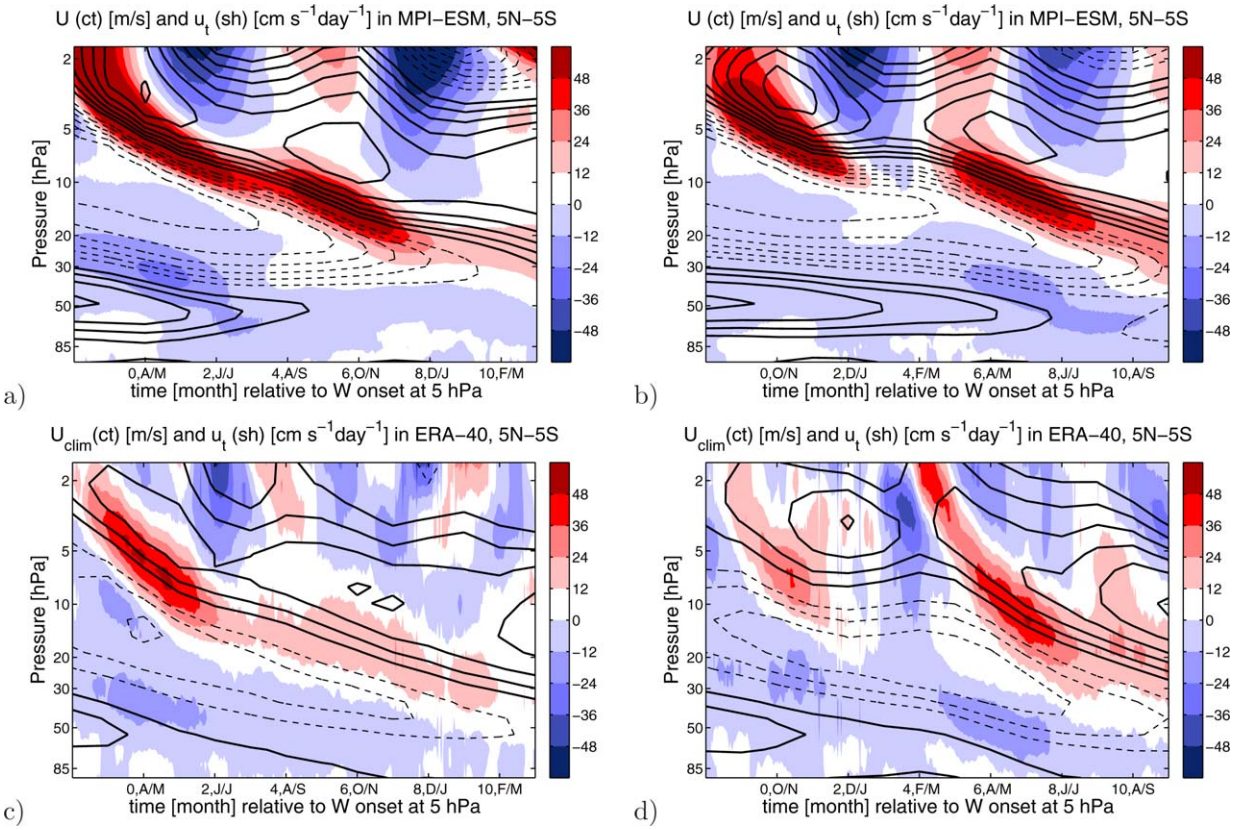

Figure 4. Time-height cross section of the composites of the zonal mean zonal wind (contour) and its acceleration (shading) in (a, b) MPI-ESM and the desasonalized zonal wind in (c, d) ERA-40. The contour interval is 5 m/s.

their momentum to the mean flow. The structure of the lower-level westerly jet is also important for resolved waves. In December/January, resolved westerly waves (phase speed $c > 0$) deposit roughly twice the momentum between 100 and 50 hPa than in June/July (Figure 5b). However, despite the strong filtering in the lower stratosphere in December/January, the peak of the resolved wave forcing of the upper QBO-westerly jet around 7 hPa is only shifted upwards by one model level and not significantly different compared to June/July (Figure 5b). The stronger resolved wave filtering at lower altitudes in December/January is compensated by a seasonal strengthening of the resolved westerly waves entering the stratosphere in winter (discussed below).

3.4. Evolution of QBO Jets in the Lower Stratosphere

[41] The difference between the structure of the lower-level westerly jets in month two of the composites in Figures 4 and 5 becomes more pronounced in later months (not shown). This is due to quick dissipation of the lower-level westerly jet in spring and summer (Figures 4a and 4c) compared to its prolonged persistence in fall and winter (Figures 4b and 4d). To which extent seasonal variations of the QBO forcing contribute to the different evolution of the lower-level QBO westerly jet is discussed next, again in the context of the momentum equation (equation (1)). However, a new set of composites has to be computed, because the weakening of the lower-level westerly jet causes a negative feedback on its forcing, as the slower jet less efficiently absorbs momentum transported by westerly waves. Sampling months with similar zonal wind profiles in the lower stratosphere excludes the dynamic feedback of the forcing and the flow and allows to discuss the seasonal variability of mean flow acceleration for a given zonal wind profile.

[42] Here, this sample consists of months when the zero-wind line between the lower-level westerly jet and the easterly jet above lies at 33 hPa. To create this sample, it has been checked in which pare of months the zonal wind at 33 hPa turns from westerly in the first month to easterly in the second month. The one of the two months where the zonal wind is closest to 0 m/s has been sampled. Such a wind reversal occurs exactly once at 33 hPa during every quasi-biennial cycle of the model run. Figure 6c shows the mean profiles of the zonal wind (black line) and vertical shear (blue line) over the selected months. The sampling criterion allows some variability of the position of zero wind lines around 33 and 86 hPa (one model level) and, more important, of the strength of the QBO westerly jet at its core around 50 hPa and of the associated vertical shear. To further

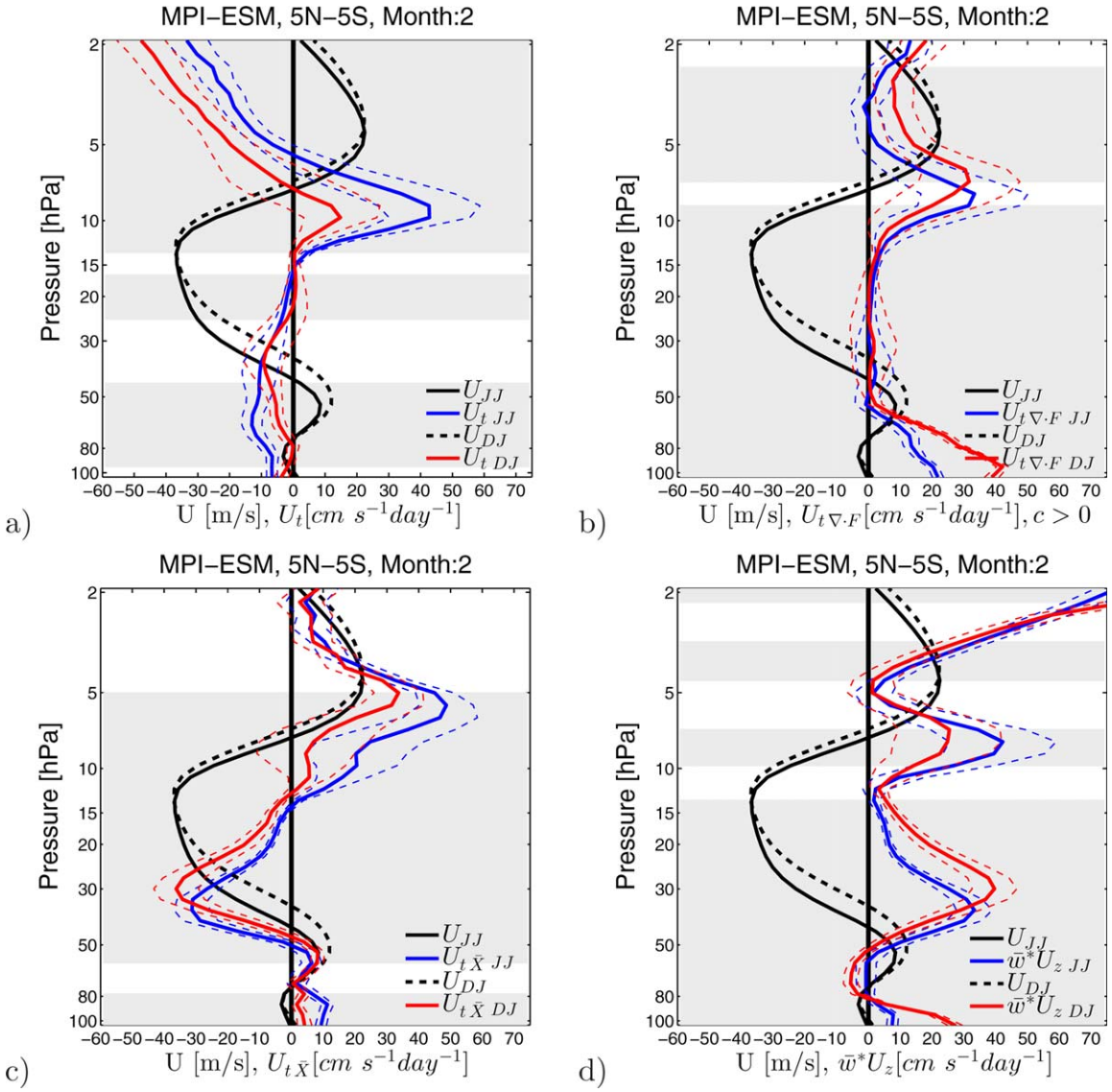

Figure 5. Profiles of the zonal mean zonal wind (m s^{-1}) 2 months after the onset of the QBO westerly jet at 5 hPa in April/May (JJ, solid black) or October/November(DJ, dashed black). The blue and red lines show (a) the respective total acceleration of the zonal wind $\overline{u}_t$, (b) the acceleration due to the resolved EP-Flux divergence from westerly waves $\overline{u}_{t\nabla\cdot F}$ ($c > 0$), (c) the parameterized wave drag and diffusion $\overline{u}_{t\overline{X}}$, and (d) the vertical momentum advection $\overline{w}^*\overline{u}_z$ in cm $s^{-1}$$day^{-1}$. The gray background indicates a statistical significant difference between the compared forcing. Dashed lines indicate ± one standard deviation.

constrain the wind profile, only those months are sampled where the wind speed at 50 hPa does not exceed the sample mean by more than ± 1.5 standard deviations. Figure 6 shows the mean values over this final 177 samples. The low standard deviations of the zonal wind and the vertical shear illustrate the strong constraint the simple sampling criterions put on the strength and vertical extent of the lower-level westerly jet. At 50 hPa, the wind speed is maximal with a sample mean of 15.4 m/s and a standard deviation of 1.1 m/s (Figure 6). At that level, the 25th and the 75th percentiles of the jet strength are 14.6 and 16.1 m/s (not shown). Hence, for MPI-ESM it was not necessary to constrain the zonal wind further. Applying the same sampling criterions on the actual zonal wind in ERA-40, the core of the lower-level QBO westerly jet has a sample mean zonal wind of 10.7 m/s with a standard deviation of 2.6 m/s and the 25th and the 75th percentiles at 9 and 13 m/s. The larger variability in ERA-40 compared to MPI-ESM is partly due to the small number of quasi-biennial cycles covered by ERA-40.

[43] To further illustrate the accuracy of the sampling method for MPI-ESM, Figure 7a shows the annual variations of the zonal wind and the shear of the selected months at 50 and 70 hPa, where the zonal wind and the shear, respectively, are strongest (Figure 6c). Both terms have an annual cycle, but vary by little more than 0.5 m/s and 0.5 m/(s km) or less than 10% of the mean

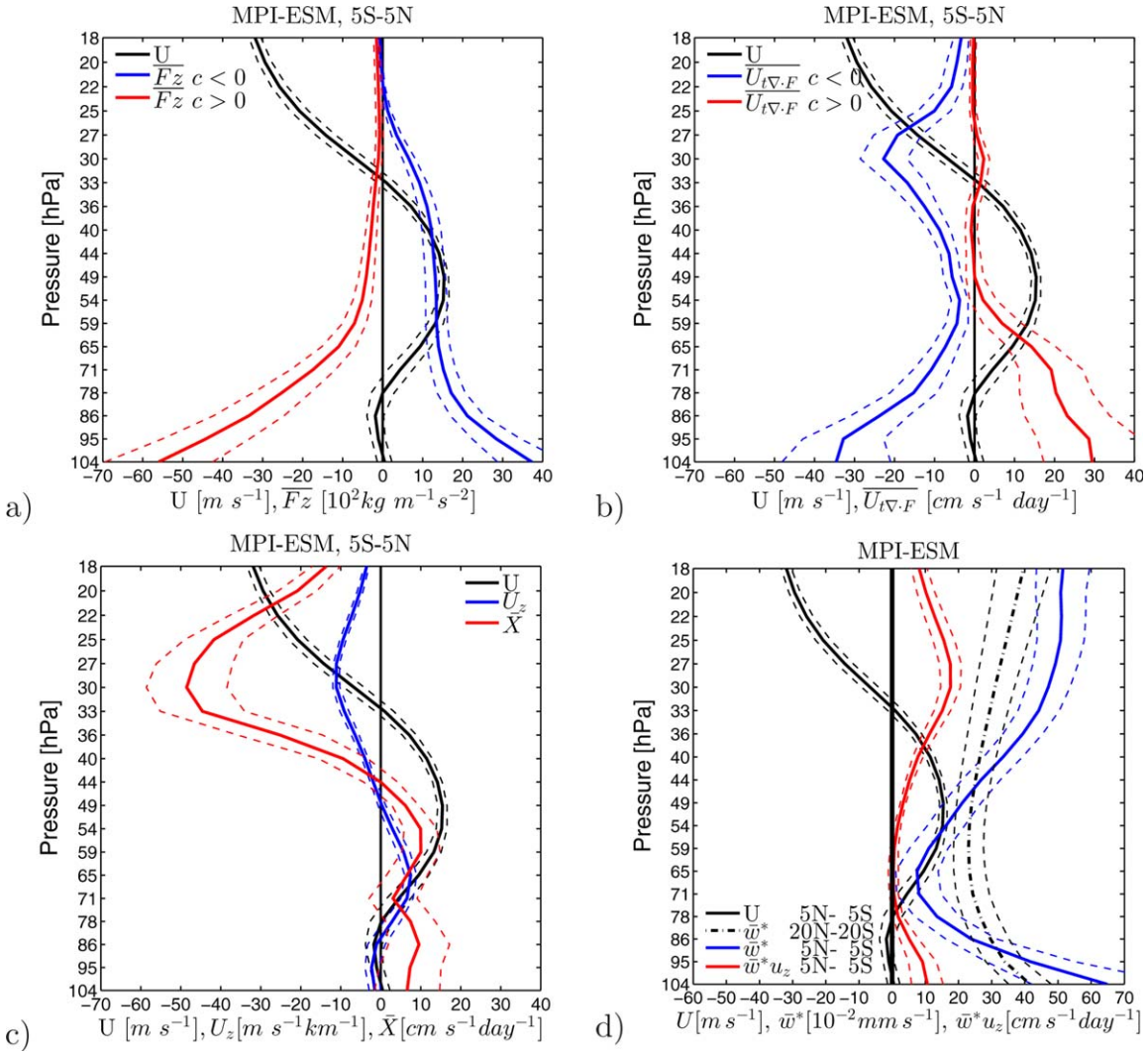

Figure 6. (a) Profile of the zonal wind in m s^{-1} (black) and the Vertical EP-Flux component in 10^2 kg $m^{-1}s^{-2}$ (F_z) of easterly (blue) and westerly waves (red) averaged from 5°S to 5°N. Dashed lines indicate ± one standard deviation. Only months when the zero-wind line between the lower-level westerly jet and the easterly jet above is located at 33 hPa are considered. (b): As Figure 6a but for the mean flow acceleration due to the divergence of the horizontal and vertical EP-Flux in cm $s^{-1}day^{-1}$ ($\overline{u}_{\nabla\cdot F}$). (c) As Figure 6a but for the mean flow acceleration due to the parameterized wave drag and diffusion in cm $s^{-1}day^{-1}$ ($\overline{X}$, red) and the vertical shear of the zonal mean zonal wind in m $s^{-1}km^{-1}$ ($\overline{u}_z$, blue). d) As Figure 6a but for the tropical and equatorial upwelling in 10^{-2}mm s^{-1} ($\overline{w}^*$, dash dotted black and blue, respectively) and the equatorial vertical momentum advection in cm $s^{-1}day^{-1}$ ($\overline{w}^*\overline{u}_z$, red). All panels show mean values over 177 samples.

values. An issue emerges when separating the selected cases into bins of the months of the year. The sample has a bias toward showing more cases in spring and summer with 58 and 42 cases in April/May and June/July, respectively, compared to 13 and 17 cases in August/September and October/November, respectively, and 30 and 17 cases in December/January and February March, respectively. This strong clustering of the QBO easterly jet's onset can also be observed in ERA-40 [*Dunkerton*, 1990]. In MPI-ESM, seasonal variations of the QBO easterly jet's descent rate, which currently are under investigation, are responsible for the strong clustering at 33 hPa compared to the broad distribution at 5 hPa (Figure 3d). However, using the same amount of cases in each bin and omitting excess months did not qualitatively change the results discussed here.

[44] To discuss the actual forcing of the lower-level westerly jet, Figure 6 also shows the sample mean profiles of the vertical EP-Flux component from easterly and westerly waves (Figure 6a), the mean flow acceleration due to resolved waves (Figure 6b) and the residual forcing term (Figure 6c). The decrease of the EP-Flux from 100 hPa to the core of the westerly jet at 50 hPa results in pronounced easterly and westerly wave forcing (Figures 6a and 6b). Above 65 hPa, the parameterized wave forcing becomes stronger than the resolved

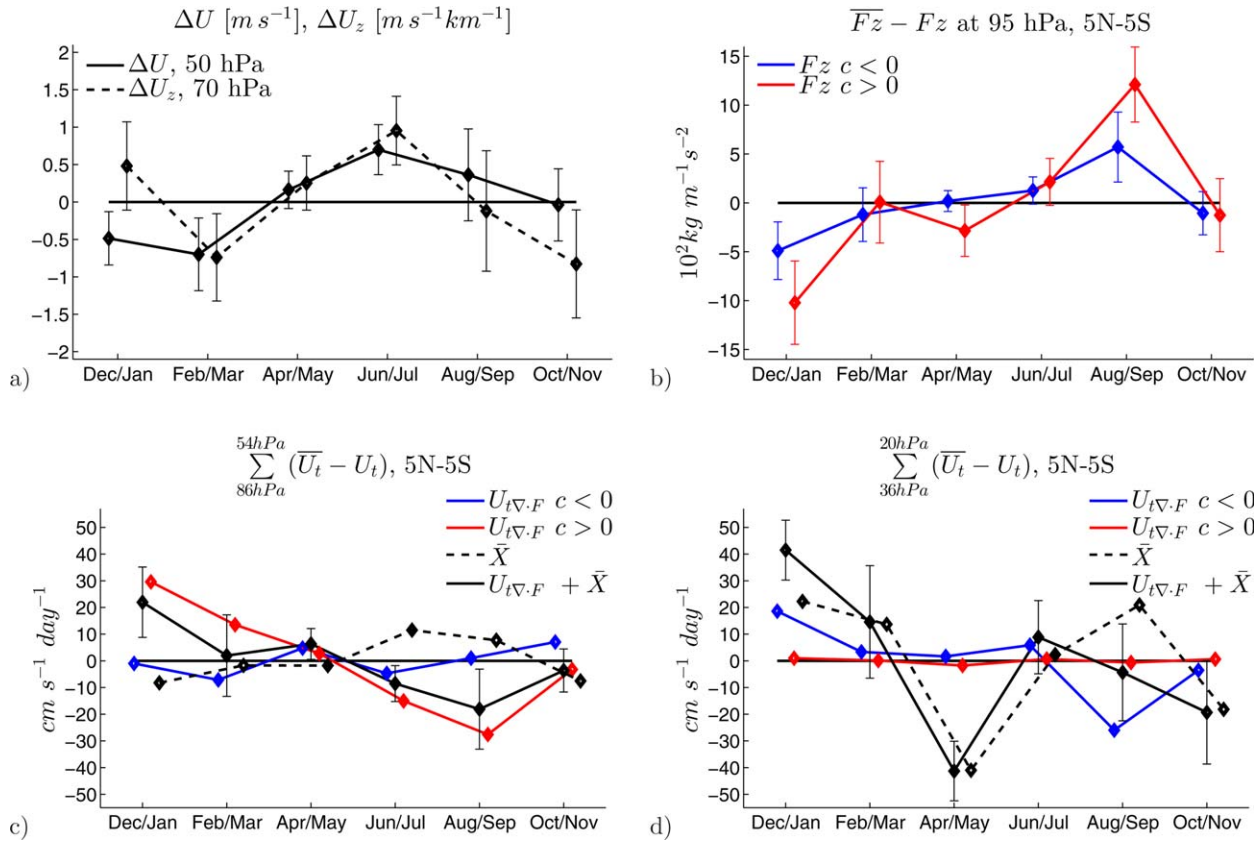

Figure 7. (a) Zonal mean wind at 50 hPa in m s^{-1} (solid) and strength of the vertical shear at 70 hPa in m $s^{-1}km^{-1}$ (dashed). (b) Vertical component of the EP-Flux due to resolved easterly (blue) and westerly waves (red) at 95 hPa. (c) and (d) Mean flow acceleration due to resolved easterly (blue) and westerly waves (red), parametrized waves and diffusion (dashed black) and their sum (solid black). The values are sums over the lower margin of the westerly jet from 86 to 54 hPa (Figure 7c) and the easterly jet from 36 to 20 hPa (Figure 7d). Errorbars indicate the 95% confidence interval. In all plots, only months when the zero-wind line between the lower-level westerly jet and the easterly jet above is located at 33 hPa are considered. The annual mean values of the selected months have been subtracted from the monthly values. In Figure 7a, positive deviations display higher wind speeds and stronger shear. In Figure 7b, negative (positive) perturbations of the EP-Flux carried by westerly (easterly) waves display stronger wave activity. In Figures 7c and 7d, positive (negative) deviations from westerly (easterly) wave forcing display stronger westerly (easterly) wave forcing. For the whole stratospheric profiles see Figure 6.

wave forcing, especially around the zero wind line at 33 hPa (cf. Figures 6b and 6c). This compares well to earlier studies of the QBO's momentum balance [*Giorgetta et al.*, 2006; *Kawatani et al.*, 2010; *Evan et al.*, 2012], which showed that small scale gravity waves are equally important for the forcing of the QBO westerly jet as large-scale equatorial waves and dominate the wave forcing of the QBO easterly jet.

[45] Figure 7 shows the quantities shown in Figure 6 sorted by the month of the year. At 95 hPa, below the region influenced by the QBO, the vertical EP-Flux from resolved westerly waves has a pronounced seasonal cycle of roughly 25% or 10^3 kg/ms^2 around the mean value (Figure 7b). Note that westerly (easterly) waves carry a negative (positive) EP-Flux (Figure 6a), and negative (positive) deviations from the mean value display stronger wave activity. Hence, the westerly wave activity is highest in December/January, and lowest in August/September (Figure 7b). The seasonal cycle of the resolved westerly wave forcing, summed over the depth of the lower-level QBO westerly jet from 86 to 54 hPa ($\pm$ 30 cm s^{-1}day^{-1}), follows the cycle of the EP-Flux (Figure 7c). The seasonal cycle of EP-Flux carried by resolved easterly waves and its mean flow acceleration are weak compared to the seasonal cycle of the westerly forcing (Figures 7b and 7c).

[46] Over the depth of the lower-level westerly jet, the residual forcing $\overline{X}$, dominated by parametrized waves, shows an annual cycle ($\pm$ 10 cm s^{-1}day^{-1}), which is out of phase with the resolved westerly wave forcing. It is strongest from June to September and weakest in December/January (Figure 7c). The parameterized wave sources are constant in time. Therefore, the annual cycle of the parameterized wave forcing is the result of wave filtering between the wave sources at 700 hPa and the lowermost stratosphere. In total, the resolved and parameterized wave forcing of the lower-

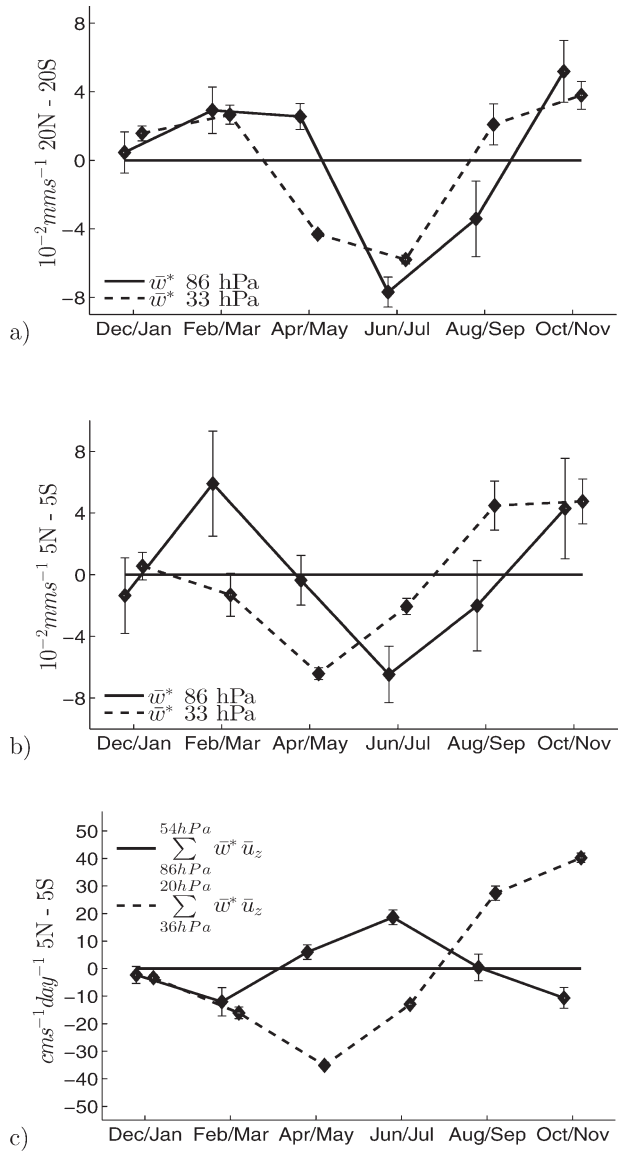

Figure 8. Seasonal variations of the vertical upwelling $\overline{w}^*$ in (a) the tropical region (20°S to 20°N) and (b) the equatorial region (5°N to 5°S). (c) Vertical advection of momentum $\overline{w}^*\overline{u}_z$ in the equatorial region. Only months when the zero wind line between the lower-level westerly jet and the easterly jet above is located at 33 hPa are considered. Values below and above the QBO westerly jet in the selected months are drawn in solid and dashed lines, respectively. The mean values shown in Figure 6d have been subtracted from the monthly values. Errorbars indicate the 95% confidence intervals.

level westerly jet is lowest from June to September and strongest in December/January (Figure 7c, black line).

[47] Not only the forcing of the lower-level westerly jet contributes to its persistence but also the drag from the QBO easterly jet, starting at 33 hPa in the selected months (Figure 6). Summed over the lower edge of the easterly jet from 36 to 20 hPa (Figures 6b and 6c), parameterized waves determine the semiannual cycle of the total wave forcing (± 40 cm $s^{-1}day^{-1}$). It is strongest (most negative) in April and May and weakest (most positive) from December to March (Figure 7d).

[48] It remains to analyze the influence of the equatorial upwelling on the evolution of the QBO jets in the lower stratosphere. Figure 6d shows the mean profiles of the equatorial and tropical residual vertical velocity and the vertical advection of momentum ($\overline{w}^*$ and $\overline{w}^*u_z$ in equation (1), respectively). The values have been averaged over 5°N to 5°S and over 20°N to 20°S for the equatorial and the tropical region, respectively. The tropical residual vertical velocity is minimal with 0.25 mm/s at 70 hPa and increases below and above (Figure 6d). The secondary circulation of the QBO [*Randel et al.*, 1998] results in lower (higher) equatorial residual vertical velocities below (above) the core of the lower-level westerly jet at 50 hPa (Figure 6d). The equatorial vertical momentum advection below and within the lower-level westerly jet is close to zero (Figure 6d). It becomes positive above 50 hPa and is strongest just above the zero-wind line of the zonal wind at 33 hPa, where the momentum advection hinders the downward propagation off the easterly jet. Figure 8 shows the annual variations of the upwelling and the momentum advection below and above the lower-level westerly jet in the selected months. At 33 hPa, the tropical upwelling has an annual cycle (Figure 8a) which is driven by the seasonal cycle of the northern hemisphere Rossby wave activity. The equatorial upwelling and vertical momentum advection, though altered by the QBO induced secondary circulation, closely follow the seasonal cycle of the tropical upwelling (Figures 8b and 8c). The resistance to the propagation of the easterly jet is strongest in late summer and fall and weakest in April/May (Figure 8c).

[49] After excluding the influence of the weakening lower-level westerly jet on the forcing, one can summarize Figures 6–8: From April to July, the lower-level westerly jet can erode quickly because the westerly wave forcing (Figure 7c), which sustains the westerly jet, and the advective resistance to the propagation of the easterly jet above the lower-level westerly jet (Figure 8c) are below their annual mean. At the same time, the wave forcing of the easterly jet (Figure 7d) is stronger than the annual mean. Later in August/September, the westerly wave forcing is weakest within the annual cycle (Figure 7c) and usually no longer capable of supporting a lower-level westerly jet, which has been weakened over spring and summer.

[50] Qualitatively, the results shown in Figures 6–8 are similar if the zero-wind line, which separates the lower-level westerly jet and the easterly jet at 33 hPa, is at lower altitudes (not shown). This allows to further discuss the evolution of the QBO jets in the lower stratosphere in MPI-ESM in Figure 4. The total zonal acceleration shown in Figures 4a and 4b is just the sum of the forcing terms shown in Figures 7c and 7d and Figure 8c for a particular wind profile. Hence, the strong easterly forcing around 33 hPa from April to July in Figures 4a and 4b (month 0–3 and 5–8, respectively) results from the seasonally strong easterly wave forcing and the weak vertical advection illustrated in Figures 7c and 8c.

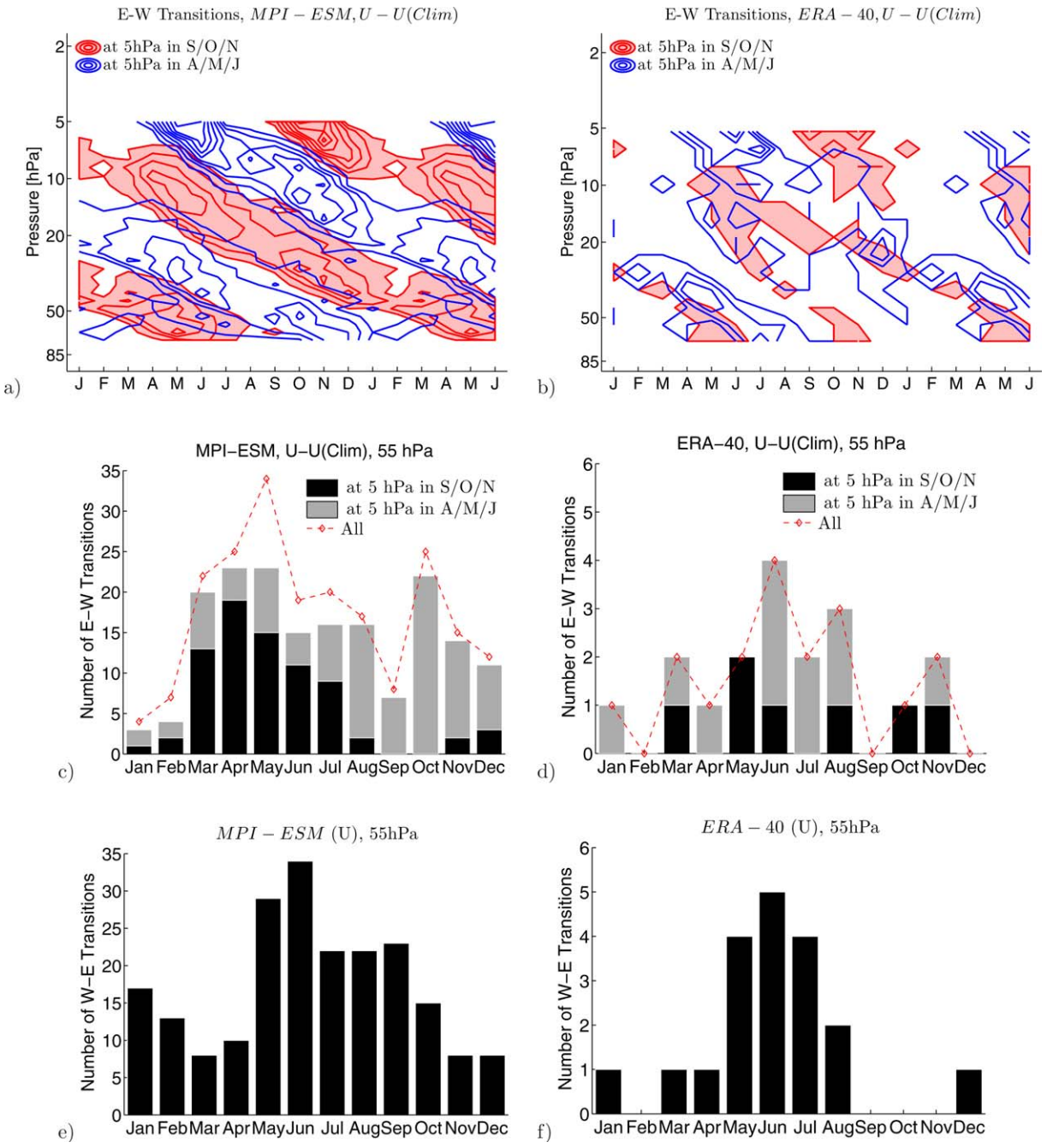

Figure 9. Distribution of the onset of the QBO westerly jets in the deseasonalized zonal wind throughout the stratosphere in (a) MPI-ESM and (b) ERA-40. The intervals are five cases for MPI-ESM and one case for ERA-40. Jets originating at 5 hPa in spring or fall are indicated in blue and red (plus shading), respectively. (c) and (d): Distribution of the onset of the QBO westerly jets in the deseasonalized zonal wind at 55 hPa in (c) MPI-ESM and (d) ERA-40. Jets originating at 5 hPa in spring and fall are indicated in gray and black, respectively. The distribution of all QBO westerly jets is drawn in dashed red. (e) and (f): Distribution of the onset of the QBO easterly jets in the zonal wind at 55 hPa in (e) MPI-ESM and (f) ERA-40.

3.5. Phase Alignment in Comparison to ERA-40

[51] After discussing seasonal differences in the evolution of the QBO westerly jets, Figures 9a and 9b show the seasonal distribution of QBO westerly jets in the deseasonalized wind initiated by the SAO at 5 hPa from April to June and from September to November throughout the stratosphere in MPI-ESM and ERA-40, respectively. The distributions shows two channel-like structures, which consist of jets initiated in spring and fall and which propagate downwards at similar rates. Seasonal peaks can be attributed to either the spring or

the fall set of jets throughout the stratosphere. This illustrates that the coupling of the QBO westerly jet's onset to the SAO at high altitudes projects on the seasonal distribution of the QBO westerly jet's onset throughout the stratosphere.

[52] Between 7 and 10 hPa, the distribution of the QBO westerly jets initiated at 5 hPa in fall (red shading in Figures 9a and 9b) shows only few occurrences from January to March. This gap in the distribution is due to the stalling of the QBO westerly jets above 7 hPa shown in Figures 4b and 4c.

[53] In MPI-ESM, the QBO westerly jets starting at 5 hPa in spring and fall cluster at 55 hPa from July to December (Figure 9c, gray bars) and from March to July (Figure 9c, black bars), respectively, and thus, are responsible for peaks in the distribution of the onset of all QBO westerly jets (Figure 9c, red curve). In ERA-40, the distribution at 55 hPa is less clear, due to the small sample size of only 18 quasi-biennial cycles (Figure 9d). However, the onset of westerly jets tends to cluster from May to August (Figure 9d, red line), mostly due to the frequent occurrence of QBO westerly jets starting at 5 hPa in spring (Figure 9d, gray bars). This shift to earlier months in ERA-40 compared to MPI-ESM indicates that QBO westerly jets starting at 5 hPa in spring propagate downwards faster in ERA-40 than in MPI-ESM.

[54] The tendency of the lower-level westerly jet to dissipate mainly during the summer months manifests in the clustering of the onset of the easterly jet. In MPI-ESM, it occurs at 55 hPa mainly between May and September, and less frequently during the rest of the year (Figure 9e). This is in good agreement with the ERA-40 data set (Figure 9f).

4. Summary and Discussion

[55] In this study, seasonal aspects of the Quasi-Biennial Oscillation in the tropical stratosphere have been investigated with a 500 year long simulation of the Max Planck Institute-Earth System Model. The model internally generates a QBO, which, compared to the ERA-40 data set, is realistic with respect to the period and vertical extent, but has a stronger amplitude.

[56] First, it has been shown that the onset of QBO westerly jets at 5 hPa mainly occurs from April to June and from September to November (section 3.2). In these months, the climatological SAO westerly jets reach the upper stratosphere. This, and the observation that every QBO westerly jet is an uninterrupted continuation of a SAO westerly jet, leads to the conclusion that the QBO westerly jets are induced by the SAO as described by previous authors [*Lindzen and Holton*, 1968; *Dunkerton*, 1997; *Kuai et al*., 2009].

[57] Theoretical and idealized model studies and tank experiments showed that QBO westerly jets can evolve in the upper stratosphere without the periodic occurrence of SAO westerly jets [*Holton and Lindzen*, 1972; *Plumb*, 1977; *Plumb and McEwan*, 1978; *Mayr et al*., 2010]. However, over the region where it is active, the westerly phase of the SAO facilitates the deposition of westerly wave momentum. When the QBO westerly jet is weak, SAO westerly jets can propagate deep into the upper stratosphere [*Dunkerton and Delisi*, 1997; *Garcia et al*., 1997; *Peña Ortiz et al*., 2010], leave the regions where periodical easterly momentum advection disturbs the westerly jet and continue as a westerly jet of the QBO.

[58] Within the sets of QBO westerly jets starting at 5 hPa in spring or fall, jets propagate downwards at similar rates (section 3.5). Thus, the seasonal clustering in the upper stratosphere extends to lower altitudes. Therefore, the coupling of the QBO westerly jet's onset to the SAO provides an explanation for the phase alignment of the QBO westerly jets found in MPI-ESM and in ERA-40 throughout the stratosphere.

[59] Second, the presented study showed that the propagation of QBO westerly jets initiated in fall in ERA-40 and MPI-ESM comes to a halt at 7 hPa during winter (Figures 4b and 4d). In MPI-ESM, this is due to variations of the equatorial upwelling and the parameterized wave forcing. In the simulation, the parametrized wave sources are constant in time. However, stronger wave filtering in the lower stratosphere and in the troposphere in winter impose the annual cycle of parameterized wave momentum reaching the stratosphere.

[60] Third, it has been shown that the observed stalling of the QBO easterly jet in the lower stratosphere in fall and winter [e.g., *Pascoe et al*., [2005], which previously has been attributed to the seasonal strengthening of the vertical upwelling [*Kinnersley and Pawson*, 1996; *Hampson and Haynes*, 2004], is supported by a seasonal weakening of the parameterized easterly wave momentum reaching the stratosphere (section 3.4). Further, the seasonal strengthening of the resolved westerly wave forcing in winter supports the QBO westerly jet in the lower stratosphere, which thus dissipates less quickly.

[61] In the future, seasonal variations of the wave activity should be investigated in simulations resolving also QBO-relevant small scale gravity waves. Further, a comparison of global climate models internally generating a QBO to find consistent features of the QBO phase alignment and the coupling to the SAO is desirable. To investigate the SAO-QBO coupling, observations with high spatial and temporal resolution in the upper stratosphere are important. However, the principal limitation of a short observational record, with a small number of observed QBO cycles remains.

[62] **Acknowledgments.** We thank two anonymous reviewers for constructive suggestions improving the paper. The MPI-ESM modeling group is acknowledged for invaluable technical support. We thank Elisa Manzini and Hauke Schmidt for fruitfull discussions. Computational resources were made available by Deutsches Klimarechenzentrum (DKRZ) through support from the Bundesministerium für Bildung und Forschung (BMBF).

References

Allen, S., and R. Vincent (1995), Gravity wave activity in the lower atmosphere: Seasonal and latitudinal variations, *J. Geophys. Res.*, *100*(D1), 1327–1350, doi:10.1029/94JD02688.

Andrews, D., J. Holton, and C. B. Leovy (1987), *Middle Atmosphere Dynamics*, 1st ed., 489 pp., Academic Press.

Anstey, J. A., and T. G. Shepherd (2008), Response of the northern stratospheric polar vortex to the seasonal alignment of QBO phase transitions, *Geophys. Res. Lett.*, *35*, 4–7, doi:10.1029/2008GL035721.

Baldwin, M. P., and L. Gray (2005), Tropical stratospheric zonal winds in ECMWF ERA-40 reanalysis, rocketsonde data, and rawinsonde data, *Geophys. Res. Lett.*, *32*, 2–6, doi:10.1029/2004GL022328.

Baldwin, M. P., et al. (2001), The quasi-biennial oscillation, *Rev. Geophys.*, *39*(2), 179–229, doi:10.1029/1999RG000073.

Delisi, D. P., and T. J. Dunkerton (1988), Seasonal variation of the semiannual oscillation, *J. Atmos. Sci.*, *45*(19), 2772–2787, doi:10.1175/1520-0469(1988)045 <2772:SVOTSO >2.0.CO;2.

Dunkerton, T. J. (1990), Annual variation of deseasonalized mean flow acceleration in the equatorial lower stratosphere, *Meteorol. Soc. Jpn.*, J., *68*(4), 499–508.

Dunkerton, T. J. (1997), The role of gravity waves in the quasi-biennial oscillation, *J. Geophys. Res.*, *102*(D22), 26,053–26,076, doi:10.1029/96JD02999.

Dunkerton, T. J., and D. P. Delisi (1985), Climatology of the equatorial lower stratosphere, *J. Atmos. Sci.*, *42*(4), 376–396, doi:10.1175/1520-0469(1985)042<0376:COTEL>2.0.CO;2.

Dunkerton, T. J., and D. P. Delisi (1997), Interaction of the quasi-biennial oscillation and stratopause semiannual oscillation, *J. Geophys. Res.*, *102*(D22), 107–116O, doi:10.1029/96JD03678.

Dunkerton, T. J., and D. Fritts (1984), Transiend gravity wave-critical layer interaction. Part I: Convectve adjustment and the mean zonal acceleration, *J. Atmos. Sci.*, *41*(6), 992–1007, doi:10.1175/1520-0469(1984)041 <0992:TGWCLI >2.0.CO;2.

Ern, M., P. Preusse, J. C. Gille, C. L. Hepplewhite, M. G. Mlynczak, J. M. Russell, and M. Riese (2011), Implications for atmospheric dynamics derived from global observations of gravity wave momentum flux in stratosphere and mesosphere, *J. Geophys. Res.*, *116*, 1–24, doi:10.1029/2011JD015821.

Evan, S., M. J. Alexander, and J. Dudhia (2012), WRF simulations of convectively generated gravity waves in opposite QBO phases, *J. Geophys. Res.*, *117*, 1–17, doi:10.1029/2011JD017302.

Fritts, D., and M. J. Alexander (2003), Gravity wave dynamics and effects in the middle atmosphere, *Rev. Geophys.*, *41*(1), 1–64, doi:10.1029/2001RG000106.

Garcia, R., T. J. Dunkerton, R. S. Lieberman, and R. A. Vincent (1997), Climatology of the semiannual oscillation of the tropical middle atmosphere, *J. Geophys. Res.*, *102*(27), 19–32, doi:10.1029/97JD00207.

Giorgetta, M. A., E. Manzini, and E. Roeckner (2002), Forcing of the quasi-biennial oscillation from a broad spectrum of atmospheric waves, *Geophys. Res. Lett.*, *29*(8), 8–11, doi:10.1029/2002GL014756.

Giorgetta, M. A., E. Manzini, E. Roeckner, M. Esch, and L. Bengtsson (2006), Climatology and forcing of the quasi-biennial oscillation in the MAECHAM5 model, *J. Clim.*, *19*, 3882–3901, doi:10.1175/JCLI3830.1.

Giorgetta, M. A., et al. (2012a), Climate change from 1850 to 2100 in MPI-ESM simulations for the coupled model intercomparison project 5, *J. Adv. Model. Earth Syst*.

Giorgetta, M. A., et al. (2012b), CMIP5 simulations of the Max Planck Institute for Meteorology (MPI-M) based on the MPI-ESM-MR model: The piControl experiment, served by ESGF, *World Data Cent. for Clim.*, doi:10.1594/WDCC/CMIP5.MXMRpc, WDCC, DKRZ .

Gray, L., and J. Pyle (1989), A two-dimensional model of the quasi-biennial oscillation of ozone, *J. Atmos. Sci.*, *46*(2), 203–220, doi:10.1175/1520-0469(1989)046 <0203:ATDMOT >2.0.CO;2.

Hamilton, K., and W. Hsieh (2002), Representation of the quasi-biennial oscillation in the tropical stratospheric wind by nonlinear principal component analysis, *J.Geophys. Res.*, *107*, 4232, doi:10.1029/2001JD001250.

Hampson, J., and P. Haynes (2004), Phase alignment of the tropical stratospheric QBO in the annual cycle, *J. Atmospheric Sci.*, *61*(21), 2627–2637, doi:10.1175/JAS3276.1.

Hines, C. O. (1997a), Doppler-spread parameterization of gravity-wave momentum deposition in the middle atmosphere. Part 1: Basic formulation, *J. Atmos. Solar-Terr. Phys.*, *59*(4), 371–386, doi:10.1016/S1364–6826(96)00079-X.

Hines, C. O. (1997b), Doppler-spread parameterization of gravity-wave momentum deposition in the middle atmosphere. Part 2: Broad and quasi monochromatic spectra, and implementation, *J. Atmos. Solar-Terr. Phys.*, *59*(4), 387–400, doi:10.1016/S1364-6826(96)00080-6.

Holton, J., and R. Lindzen (1972), An updated theory for the quasi-biennial cycle of the tropical stratosphere, *J. Atmos. Sci.*, *29*(6), 1076–1080, doi:10.1175/1520-0469(1972)029 <1076:AUTFTQ >2.0.CO;2.

Holton, J., and H. Tan (1980), The influence of the equatorial quasi-biennial oscillation on the global circulation at 50 mb, *J. Atmos. Sci.*, *37*(10), 2200–2208, doi:10.1175/1520-0469(1980)037 <2200:TIOTEQ >2.0.CO;2.

Horinouchi, T., et al. (2003), Tropical cumulus convection and upward-propagating waves in middle-atmospheric GCMs, *J. Atmos. Sci.*, *60*, 2765–2782, doi:10.1175/1520-0469(2003)060 <2765:TCCAUW >2.0.CO;2.

Kawatani, Y., S. Watanabe, K. Sato, T. J. Dunkerton, S. Miyahara, and M. Takahashi (2010), The roles of equatorial trapped waves and internal inertiagravity waves in driving the quasi-biennial oscillation. Part I: Zonal mean wave forcing, *J. Atmos. Sci.*, *67*(4), 963–980, doi:10.1175/2009JAS3222.1.

Kinnersley, J., and S. Pawson (1996), The descent rates of the shear zones of the equatorial QBO, *J. Atmos. Sci.*, *53*(14), 1937–1949, doi:10.1175/1520-0469(1996)053 <1937:TDROTS >2.0.CO;2.

Kuai, L., R.-L. Shia, X. Jiang, K.-K. Tung, and Y. L. Yung (2009), Nonstationary synchronization of equatorial QBO with SAO in observations and a model, *J. Atmos. Sci.*, *66*(6), 1654–1664, doi:10.1175/2008JAS2857.1.

Li, T., T. Leblanc, I. S. McDermid, D. L. Wu, X. Dou, and S. Wang (2010), Seasonal and interannual variability of gravity wave activity revealed by long-term lidar observations over Mauna Loa Observatory, Hawaii, *J. Geophys. Res.*, *115*, D13103, 1–10, doi:10.1029/2009JD013586.

Lindzen, R., and J. Holton (1968), A Theory of the quasi-biennial oscillation, *J. Atmos. Sci.*, *25*, 1095–1107, doi:10.1175/1520-0469(1972)029 <1076:AUTFTQ >2.0.CO;2.

Lu, B.-W., L. Pandolfo, and K. Hamilton (2009), Nonlinear representation of the quasi-biennial oscillation, *J. Atmos. Sci.*, *66*(7), 1886–1904, doi:10.1175/2008JAS2967.1.

Manzini, E., and N. a. McFarlane (1998), The effect of varying the source spectrum of a gravity wave parameterization in a middle atmosphere general circulation model, *J. Geophys. Res.*, *103*(D24), 31,523–31,539, doi:10.1029/98JD02274.

Manzini, E., M. a. Giorgetta, M. Esch, L. Kornblueh, and E. Roeckner (2006), The Influence of Sea Surface Temperatures on the Northern Winter Stratosphere: Ensemble Simulations with the MAECHAM5 Model, *J. Clim.*, *19*(15), 3863–3881, doi:10.1175/JCLI3826.1.

Marsland, S., H. Haak, J. Jungclaus, M. Latif, and F. Röske (2003), The Max-Planck-Institute global ocean/sea ice model with orthogonal curvilinear coordinates, *Ocean Modell.*, *5*(2), 91–127, doi:10.1016/S1463-5003(02)00015-X.

Mayr, H., J. Mengel, K. Chan, and F. Huang (2010), Middle atmosphere dynamics with gravity wave interactions in the numerical spectral model: Zonal-mean variations, *J. Atmos. Solar-Terr. Phys.*, *72*, 807–828, doi:10.1016/j.jastp.2010.03.018.

Naujokat, B. (1986), An update of the observed quasi-biennial oscillation of the stratospheric winds over the tropics, *J. Atmos. Sci.*, *43*(17), 1873–1877, doi:10.1175/1520-0469(1986)043 <1873:AUOTOQ >2.0.CO;2.

Nordeng, T. E. (1996), Extended versions of the convective parameterization scheme at ECMWF and their impact on the mean and transient activity of the model in the tropics, *ECMWF Research Dep. Techn. Memo 206*, ECMWF, Reading.

Pascoe, C. L., L. Gray, S. A. Crooks, M. N. Juckes, and M. P. Baldwin (2005), The quasi-biennial oscillation: Analysis using ERA-40 data, *J. Geophys. Res.*, *110*, 1–13, doi:10.1029/2004JD004941.

Peña Ortiz, C., P. Ribera, R. García-Herrera, M. A. Giorgetta, and R. R. García (2008), Forcing mechanism of the seasonally asymmetric quasi-biennial oscillation secondary circulation in ERA-40 and MAECHAM5, *J. Geophys. Res.*, *113*, 1–16, doi:10.1029/2007JD009288.

Peña Ortiz, C., H. Schmidt, M. A. Giorgetta, and M. Keller (2010), QBO modulation of the semiannual oscillation in MAECHAM5 and HAMMONIA, *J. Geophys. Res.*, *115*, 1–19, doi:10.1029/2010JD013898.

Plumb, R. (1977), The interaction of two internal waves with the mean flow: Implications for the theory of the quasi-biennial oscillation, *J. Atmos. Sci.*, *34*(12), 1847–18,598, doi:10.1175/1520-0469(1977)034 <1847:TIOTIW >2.0.CO;2.

Plumb, R., and A. McEwan (1978), The instability of a forced standing wave in a viscous stratified fluid: A laboratory analogue of the quasi-biennial oscillation, *J. Atmos. Sci.*, *35*, 1827–1839, doi: 10.1175/1520-0469(1978)035 <827:TIOAFS >2.0.CO;2.

Punge, H. J., and M. A. Giorgetta (2007), Differences between the QBO in the first and in the second half of the ERA-40 reanalysis, *Atmos. Chem. Phys.*, *7*(2005), 599–608, doi:10.5194/acp-7-599-2007.

Raddatz, T. J., C. H. Reick, W. Knorr, J. Kattge, E. Roeckner, R. Schnur, K.-G. Schnitzler, P. Wetzel, and J. Jungclaus (2007), Will the tropical land biosphere dominate the climatecarbon cycle feedback during the twenty-first century? *Clim. Dyn.*, *29*(6), 565–574, doi:10.1007/s00382-007-0247-8.

Randel, W., F. Wu, J. M. Russell, A. Roche, and J. Waters (1998), Seasonal cycles and QBO variations in stratospheric CH 4 and H 2 O observed in UARS HALOE data, *J. Atmos. Sci.*, *55*(2), 163–185, doi:10.1175/1520-0469(1998)055 <0163:SCAQVI >2.0.CO;2.

Scaife, A. A., N. Butchart, and C. D. Warner (2000), Realistic Quasi-Biennial Oscillations in a simulation of the global climate, *Geophys. Res. Lett.*, *27*(1), 3481–3484, doi:10.1029/2000GL011625.

Schmidt, H., et al. (2012), The response of the middle atmosphere to anthropogenic and natural forcing in the CMIP5 simulations with the MPI-ESM, *J. Adv. Model. Earth Syst*., doi:10.1002/jame.20014.

Stevens, B., et al. (2012), The atmospheric component of the MPI-ESM: ECHAM6, *J.Adv. Model. Earth Syst*., doi:10.1002/jame.20015, in press.

Takahashi, M. (1999), Simulation of the quasi-biennial oscillation in a general circulation model, *Geophys. Res. Lett.*, *26*(9), 1307–1310, doi:10.1029/1999GL900188.

Tiedtke, M. (1989), A comprehensive mass flux scheme for cumulus parameterization in large- scale models, *Mon. Weather Rev.*, *117*(8), 1779–1800, doi:10.1175/1520-0493(1989)117 <1779:ACMFSF >2.0.CO;2.

Wallace, J. M., R. L. Panetta, and J. Estberg (1993), Representation of the equatorial stratsopheric quasi-biennial oscillation in EOF phase space, *J. Atmos. Sci.*, *50*(12), 1751–1762, doi:10.1175/1520-0469(1993)050 <1751:ROTESQ >2.0.CO;2.

Yang, G.-Y., B. Hoskins, and L. Gray (2012), The Influence of the QBO on the propagation of equatorial waves into the stratosphere, *J. Atmos. Sci.*, *69*(10), 2959–2982, doi:10.1175/JAS-D-11-0342.1.

Corresponding author. T. R. Krismer, Max Planck Institute for Meteorology, Bundesstr. 53, 20146 Hamburg, Germany. (thomas.krismer@zmaw.de)